Energy-Conscious Warm-Up of Li-ion Cells From Sub-Zero Temperatures

Shankar Mohan, Youngki Kim, *Member, IEEE,* and Anna G. Stefanopoulou, *Fellow, IEEE*

***Abstract*—Lithium (Li) ion battery cells suffer from significant performance degradation at sub-zero temperatures. This paper presents a Predictive Control based technique that exploits the increased internal resistance of Li-ion cells at sub-zero temperatures to increase the cell's temperature until the desired power can be delivered. Specifically, the magnitude of a sequence of bidirectional currents is optimized such as to minimize total energy discharged. The magnitude of current is determined by solving an optimization problem that satisfies the battery manufacturer's voltage and current constraints. Drawing bi-directional currents necessitates that a temporary energy reservoir for energy shuttling, such as an ultra-capacitor or another battery, be available. When compared with the case when no penalty on energy withdrawn is imposed, simulations indicate that reductions of up to 20% in energy dispensed as heat in the battery as well as in the size of external storage elements can be achieved at the expense of longer warm-up operation time.**

***Index Terms*—Lithium-ion batteries, battery management, low-temperature operation, warm-up, model predictive control, Hybrid Electric Vehicle**

I. Introduction

THE use of Li-ion battery technologies has recently enjoyed widespread adoption in consumer electronics and automotive/aerospace applications [1]. The archetype of rechargeable technology, Li-ion batteries, has over the last decade benefited from improvements in material science through increased energy and power density [2]. Although widely adopted, these batteries suffer from significant performance degradation at low temperatures ($\leq -10^o$C) posing a challenge for automotive applications (refer [3] and [4] for electrochemistry based reasons).

Although improvement to sub-zero performance through changes in design and construction of cells have been pursued, the need for fast warm-up is relevant for existing equipments. Battery warm-up techniques can be broadly classified as – (1) jacket/resistive/external heat-up; (2) internal heating using high-frequency bidirectional currents. In [5], various methods to use convective heating of cells/packs using air and phase change materials is surveyed. More recently, in [6], the authors study the use of phase change slurry to externally warm the pack and in [7] the authors use power electronics to place air heaters in parallel (power) to the motors in Electric Vehicles (EVs) to warm the battery pack. Pesaran *et.al.* in [8] and Stuart *et.al.* in [9] studied the use of bi-directional sinusoidal high frequency current to increase the cell's temperature through internal heating. In Ji *et al.* in [10] compare different heating strategies and conclude that for Li-ion cells, internal heating is more effective than using external heating elements if no external power source is utilized, a scenario we term as *standalone* and is of consideration in this paper.

Most techniques discussed in literature strive to warm the cell until a certain pre-specified cell temperature is reached. Since in most applications, the cell serves as a source of power, we use the cell's pulse power capability, instead of the temperature, as a condition to terminate the warm-up operation. In addition, we seek to investigate the feasibility of reaching the necessary power capability in an energy efficient manner.

Pulse power capability or state-of-power (SOP) is an estimated quantity whose accuracy is determined by the fidelity of the model that captures the electrical dynamics of the cell [11]. Modeling the electrical behavior of Li-ion cells at sub-zero temperatures, particularly at high current rates, is more challenging than emulating its thermal dynamics [4]. Thus, owing to the inherent relation between operating temperature and power capability, in this paper, temperature rise is taken as a measurable surrogate. Then, the stated objective of increasing power capability can be re-written as one of effecting temperature rise in an energy conscious manner *until* the desired power can be delivered.

Maximizing temperature rise while regulating energy loss provides for certain desirable characteristics of the battery current. Heat generated being proportional to the input current, it follows that the candidate current profile be bi-directional to minimize cumulative discharge and achieve fast warm-up. Drawing bi-directional currents necessitates that a temporary energy reservoir for energy shuttling, such as an ultra-capacitor or another battery, be available. Since the bi-directional current includes a charging phase, it is important to note that charging the cell at low temperatures is challenging and imposes stringent charging current constraints (see [12], [13] for challenges at room temperature).

Charging Li-ion cells at sub-zero temperatures is difficult because of the reduced diffusivity in the anode that results in increased polarization and a drop in electrode overpotential [14], [15]. From a control perspective, the propensity of charging currents to cause plating can be minimized by actively

Manuscript received October 12, 2014; revised March 16, 2015 and July 1, 2015; accepted September 9, 2015.

This work was supported by the Automotive Research Center through the U.S. Army Tank Automotive Research, Development and Engineering Center, Warren, MI, USA, under Grant W56HZV-04-2-0001.

S. Mohan is with the Department of Electrical Engineering and Computer Science, University of Michigan, Ann Arbor, MI 48109 USA (e-mail: elemsn@umich.edu).

Y. Kim and A. G. Stefanopoulou are with the Department of Mechanical Engineering, University of Michigan, Ann Arbor, MI 48109 USA (e-mail: youngki@umich.edu; annastef@umich.edu).

This article has been accepted for publication in a future issue of this journal, but has not been fully edited. Content may change prior to final publication. Citation information: DOI 10.1109/TIE.2016.2523440, IEEE Transactions on Industrial Electronics

regulating the electrode overpotential. Pulsed charging is one of the most widely adopted technique to slow down polarization and allow for more even ion distribution [16]. In this paper, in addition to using bi-directional pulses, anode polarization is indirectly controlled by enforcing the magnitude of charging currents to be less than the discharging portion of the pulse.

This paper attempts to study the feasibility of using computationally efficient models to improve the power capability of Li-ion cells in an energy efficient manner. This paper is organized as follows. The models that are used to mimic the cell's electrical and thermal behavior are detailed in Section II and their parametrization is discussed in Section III. The control problem is formulated in Section IV and an example simulation is studied in Section V. Conclusions and final remarks are made in Section VI.

II. Modeling

This section introduces the models of electrical and thermal dynamics adopted in this study. The dynamic behavior of a cylindrical (26650) LFP cell is captured using simple reduced order models. The validity of the chosen models for the application at hand is ascertained through experimental validation.

A. Electrical Model

Over the decades, much effort has been expended in developing phenomenological models of the electrical dynamics. The more complex models are based on concentration theory, first proposed by Doyle, Fuller and Newman in [17]. Models so derived are hard to parameterize [18], have notable memory requirements and, are computationally intensive. On the other hand, equivalent circuit models have been widely adopted in literature and in practice, eg. [19] and references therein.

Small signal and local approximations of the dynamic behavior of electrochemical studies can be obtained by using impedance measurements [20]. Results of the impedance spectroscopy study conducted in [21] suggest that at low operating temperatures, for high frequencies of current, the Li-ion cell's electrical dynamics exhibits a first order characteristic. Thus, in this paper, an equivalent circuit model whose dynamics is governed by Eqn. (1) is utilized to capture the electrical dynamics of the Li-ion cell. Note that the system Eqn. (1) describes is one of a Linear Parameter Varying system wherein the parameters are scheduled based on the state of charge (SOC), z, and the cell temperature T

$$\underbrace{\begin{bmatrix}\dot{z}\\ \dot{V}_1\end{bmatrix}}_{x_{el}} = \underbrace{\begin{bmatrix}0 & 0\\ 0 & -\dfrac{1}{R_1(\cdot)C_1(\cdot)}\end{bmatrix}}_{A_{el}}\begin{bmatrix}z\\ V_1\end{bmatrix} + \underbrace{\begin{bmatrix}-\dfrac{1}{3600\cdot C_b(T)}\\ -\dfrac{1}{C_1(\cdot)}\end{bmatrix}}_{B_{el}} v_{el},$$

$$V_t = V_{OCV}(z,T) - V_1 - R_s(\cdot)v_{el}. \tag{1}$$

where $v_{el} = I$ (sign convention – charge : negative; discharge : positive), C_b is the temperature dependent capacity of the cell; V_t is the terminal voltage of the cell; V_{OCV} is the Open Circuit Voltage (OCV), a function of SOC and cell temperature; and $R_s(\cdot)$ is the series resistance. Figure 1 presents

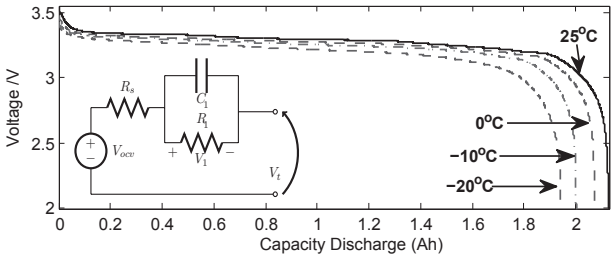

Fig. 1. Relation between temperature, OCV and capacity, (inset) single R-C equivalent circuit representation of electrical dynamics

an electric equivalent of the dynamical system in Eqn (1) and the dependence of C_b on temperature. State V_1 can be interpreted as being indicative of the bulk polarization in the cell; its time constant is determined by the pair $\{R_1, C_1\}$ which is assumed to be a function of SOC, cell temperature and current direction. In the interest of notational simplicity, in the remainder of the paper, the dependence of model parameters on dynamic states and input is not explicitly stated when there is little room for confusion.

The power capability of a cell is defined as the product of the maximum continuous current that can be drawn over a fixed time interval without violating current and or voltage constraints. In this paper, estimates of power capability for a pulse duration of N samples are computed in discrete-time using expressions provided in [22]. In discrete-time domain, denoting the linearized system matrices of the electrical model as A^d_{el}, B^d_{el}, C^d_{el}, D^d_{el},

$$P_{cap,k} = V_{min}\left\{\frac{V_{min} - V_{OCV}(z_k) + C^d_{el}Lz_k - C^d_{el}(A^d_{el})^N x_{el,k}}{C^d_{el}M^d_{el} + D^d_{el}}\right\}, \tag{2}$$

where V_{min} is the minimum permissable terminal voltage, $L = [1,\, 0,\, 0]'$, $M = \sum_{i=0}^{N-1}(A^d_{el})^j B^d_{el}$ and N is the number of samples in the constant discharge pulse.

B. Thermal Model

The thermal model of a cylindrical battery developed in [23] is taken to represent the thermal dynamics in this study. The model of the thermal dynamics when expressed in terms of the core (T_c), surface (T_s), ambient (T_{amb}) temperatures and rate of heat generation (q) is represented as

$$\begin{aligned}\dot{x}_{th} &= A_{th}x_{th} + B_{th}v_{th},\\ y_{th} &= C_{th}x_{th} + D_{th}v_{th},\end{aligned} \tag{3}$$

TABLE I
Thermal Model Parameters

Parameter	Symbol	Value	Unit
Density	ρ	2047	kg/m^3
Specific heat coeff.	c_p	1109	J/kgK
Thermal conductivity	k_t	0.610	W/mK
Radius	r	12.9×10^{-3}	m
Height	L	65.15×10^{-3}	m
Volume	v_b	3.421×10^{-5}	m^3

where the states represent temperature gradient across the radius ($\bar{\gamma}$) and average temperature ($\bar{T}$); $x_{th} = [\bar{T}\ \bar{\gamma}]^T$, $v_{th} = [q\ T_{amb}]^T$ and $y_{th} = [T_c\ T_s]^T$. System matrices A_{th}, B_{th}, C_{th}, and D_{th} are defined as follows:

$$A_{th} = \begin{bmatrix} \frac{-48\alpha h}{r(24k_{th}+rh)} & \frac{-15\alpha h}{24k_{th}+rh} \\ \frac{-320\alpha h}{r^2(24k_{th}+rh)} & \frac{-120\alpha(4k_{th}+rh)}{r^2(24k_{th}+rh)} \end{bmatrix},$$

$$B_{th} = \begin{bmatrix} \frac{\alpha}{k_{th}V_b} & \frac{48\alpha h}{r(24k_{th}+rh)} \\ 0 & \frac{320\alpha h}{r^2(24k_{th}+rh)} \end{bmatrix},$$

$$C_{th} = \begin{bmatrix} \frac{24k_{th}-3rh}{24k_{th}+rh} & -\frac{120rk_{th}+15r^2h}{8(24k_{th}+rh)} \\ \frac{24k_{th}}{24k_{th}+rh} & \frac{15rk_{th}}{48k_{th}+2rh} \end{bmatrix},$$

$$D_{th} = \begin{bmatrix} 0 & \frac{4rh}{24k_{th}+rh} \\ 0 & \frac{rh}{24k_{th}+rh} \end{bmatrix}, \quad (4)$$

where k_{th}, h and ρ are the thermal conductivity, convection coefficient and bulk density, α, the thermal diffusivity is defined as the ratio of k_{th} to the heat capacity, c_p. These parameters are assumed to independent of the cell and ambient temperatures.

The bulk of heat generation in electrochemical cells can be attributed to three components – Joule, entropic and heating due to polarization. Since the current in this application is bidirectional and is large in magnitude, Joule heating dominates entropic heating. Further, the heat generated by polarization is affected by the time constant of the R-C pair and the voltage across them.

$$q = \frac{V_1^2}{R_1} + I^2 R_s \quad (5)$$

III. Model Parametrization & Validation

The parameters of the thermal model, thermal properties of the cell and the environment, are not significantly influenced by temperature variations. This affords us the option of adopting values presented in [23] (reproduced in Table I) without change. However, a similar argument cannot be made for the electrical model.

Modeling the electrical dynamics of Li-ion cells as a linear parameter varying system has been extensively pursued in literature eg. [19] and references therein. In this paper, the standard method utilized to parameterize equivalent circuit models and which is described in [19] is extended to sub-zero temperatures.

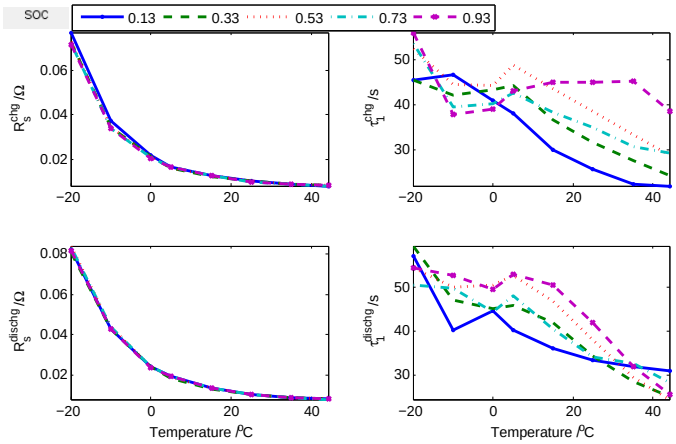

Fig. 2. Estimated SOC and temperature dependent parameters at different SOCs during charge (chg) discharge ($dischg$)

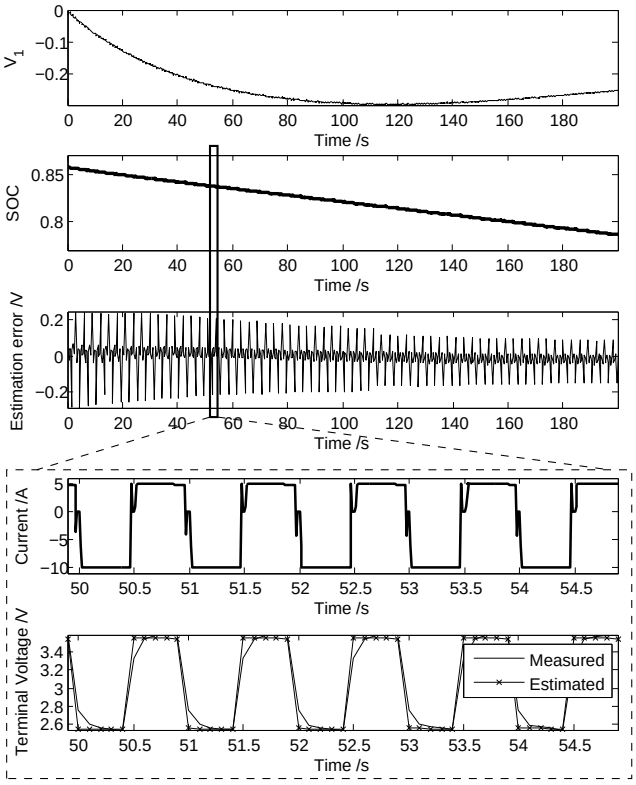

Fig. 3. Model validation – Predicting Terminal Voltage

Figure 2 presents some of the key characteristics of the representative sub-model; each line in every subplot corresponds to the trajectory of the variable as a temperature changes for a particular SOC.

Based on the estimated values for model parameters, for large currents, it can be shown that the heat generated can be approximated by Joule heating. Hence in the remainder of the paper, the generated heat is computed as

$$q = I^2 R_s. \quad (6)$$

To validate the models described in the sections afore, a 26650 LFP cell was instrumented with a thermocouple in its center cavity and placed in a Cincinnati Sub-Zero ZPHS16-3.5-SCT/AC temperature controlled chamber. The chamber temperature was set to -20 °C and the air-flow was regulated to mimic natural convection ($h = 5\ W/m^2K$). This cell was excited with square current pulse-train provided by a Bitrode FTV1-200/50/2-60 cycler. Each pulse in current was set to have a duty-cycle of 50% and the magnitude of charging and discharging currents were set at five and 10 amperes. The frequency of pulse-train was set to 1 Hz and measurements of terminal voltage, current, surface and core temperature were collected at the rate of 100 Hz. The measured current was fed to both the electrical (single R-C model) and thermal models and the estimated terminal voltage, surface and core temperatures are plotted in Figs. 3 – 4.

This article has been accepted for publication in a future issue of this journal, but has not been fully edited. Content may change prior to final publication. Citation information: DOI 10.1109/TIE.2016.2523440, IEEE Transactions on Industrial Electronics

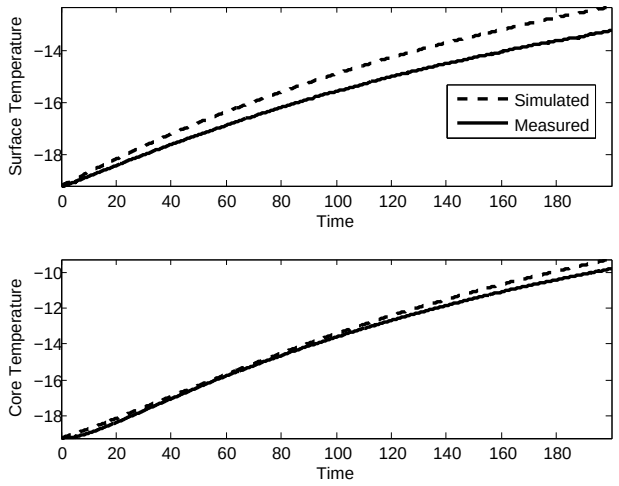

Fig. 4. Model Validation – Predicting Surface and Core temperatures

From Fig. 3 it is noted that the root mean squared (rms) error in estimating the terminal voltage is less than 50 mV. Much of the large errors in estimation of terminal voltage is incident with changes in current direction. The most likely reason is that while the model is able to capture the steady state values, it has deficiencies in capturing the very fast transients. The relatively slower transients are captured by the R-C pair in the model and the first subplot in Figure 3 traces the trajectory of the estimated bulk polarization. Observe that the polarization voltage is at-times almost 10% of the total voltage swing across the entire SOC range and can can significantly the measured terminal voltage.

In this work, we are interested in warming the cell. Since most of the heat is generated through Joule heating and given that the parameterized model is able to capture the steady-state voltage fairly accurately, the developed model is assumed adequate and is used in the remainder of the paper.

Figure 4 presents the outcome of simulating the thermal model. The input to the thermal model, namely Joule heating, was computed using the electrical model parameters and states. Upon inspection, it is possible to conclude that the thermal model is able to predict the surface and core temperatures to within the accuracy of the T-junction thermocouples, 0.5°C, for the critical range of cold conditions

IV. Automated optimal warm-up formulation

The primary focus of this work is on warming the cell in an energy efficient manner until the desired power can be drawn from the cell. To this end, based on electrochemical considerations, the profile of input current is chosen as a sequence of bi-directional pulses recurring at a certain frequency. To keep the problem formulation simple, each period is stipulated to have just one sign change in current as shown in Figure 5. To completely characterize the current profile, one would require four control variables – frequency, duty-cycle, peaks of charge and discharge pulses. The frequency of the pulse train influences the rate of heat generation – from EIS tests, increasing frequencies decreases the effective series resistance while decreasing the reactive component of the total impedance [24]. In this study, the optimal frequency at which the resistance is *large* yet the reactive component is *small* is assumed to be known. Since the frequency is pre-determined, the values of the remaining variables – duty-cycle and magnitudes, need to be determined.

The dynamic behavior of the electrical and thermal sub-systems of the cell are functions of its operating conditions and internal states. Specifically, the optimal decision at the kth instance is influenced by the trajectory of states until then. As the model dynamics is affected by the value of its states, the problem of deciding the values of the control variables is formulated as a linearized receding finite horizon optimization problem and described in this section.

The objective of the problem under consideration is to increase the temperature of the cell while penalizing the effective energy discharged (measured in terms of loss in SOC) from the cell. This objective can, in the general case, be mathematically formulated as

$$\min_{\mathcal{U},\mathcal{D}} \; -[\bar{T}_{k+1+n_s\cdot N} - \bar{T}_{k+1}] + \tilde{\beta}\sum_{j=1}^{N}(u_{c,j}\cdot d_{c,j} + u_{d,j}\cdot d_{d,j}), \tag{7}$$

where N is the number of periods in prediction horizon, $\tilde{\beta}$ is the relative penalty on energy loss, n_s is the number of samples per period of the pulse; in the j^{th} period of the horizon, $d_{c,j}$ and $d_{d,j}$ are the durations of charge and discharge portion of the period as multiples of sampling period ΔT, and $u_{c,j}$ and $u_{d,j}$ are the the charge and discharge currents. Then,

$$\mathcal{D} = \big\{\{d_{c,j},\, d_{d,j}\} \mid \forall j \in [1,N]\cap\mathbb{Z},\, d_{c,j}+d_{d,j}\le n_s\big\},$$
$$\mathcal{U} = \big\{\{u_{c,j},\, u_{d,j}\} \mid \forall j \in [1,N]\cap\mathbb{Z},\, |u_{c,j}|\le |u_{d,j}|\big\}.$$

Note that Eqn. (7) is, by virtue of the fact that the second term is non-convex and that the first and second terms do not have terms in common, non-convex. The variables over which the problem is optimized takes a mixture of integer and continuous values; the problem under consideration is a non-convex Mixed Nonlinear Integer Programming problem (MNIP). Non-convex MNIPs are NP-hard [25] and are not suitable for online control. In the interest of making the problem more tractable, in this paper, the duty-cycle of both charge and discharge pulses are set to be equal; i.e. 50% duty-cycle; in so doing, the problem

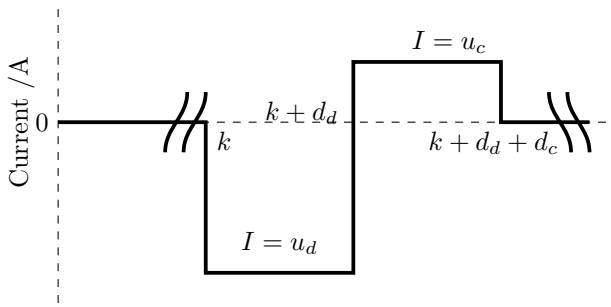

Fig. 5. Pulse current profile

This article has been accepted for publication in a future issue of this journal, but has not been fully edited. Content may change prior to final publication. Citation information: DOI 10.1109/TIE.2016.2523440, IEEE Transactions on Industrial Electronics

devolves into a regular nonlinear programming problem (NLP) that could be solved online.

Having fixed the duty-cycle to be 50%, for simplicity of expressions, without loss of generality it is assumed that each period of the current is spread over only two samples. A more general case is easily derived by scaling the appropriate variables.

A. Characterizing the Current Profile

At each instant l, for a prediction horizon of length $2N$ samples, the problem of deciding the magnitude of pulses to increase cell temperature in an energy conscious manner is computed by solving the following problem **P1**:

$$\begin{aligned}
&\min_{u} \; -[\bar{T}_{l+2N+1} - \bar{T}_{l+1}] + \tilde{\beta}|z_{l+2N+1} - z_{l+1}| \\
&\text{s.t. : } \forall k \in \{l+0, \ldots, l+2N\} \\
&\left.\begin{aligned} x_{th,k+1} &= A^d_{th}x_{th,k} + B^d_{th}v_{th,k} \\ y_{th,k} &= C^d_{th}x_k + D^d_{th}v_{th,k} \\ v_{th,k} &= [u_k^2 R_{s,k}; T_{amb,k}] \end{aligned}\right\} \quad (8a) \\
&\left.\begin{aligned} x_{el,k+1} &= A^d_{el}x_{el,k} + B^d_{el}u_k \\ y_{el,k} &= C^d_{el}x_{el,k} + D^d_{el}u_k + G^d_{el} \end{aligned}\right\} \quad (8b) \\
&\left.\begin{aligned} |u_i| &\le |I_d(\bar{T}_i)|, \forall i \in \{l+1, l+3, \ldots, l+2N-1\} \\ |u_i| &\le |I_c(\bar{T}_i)|, \forall i \in \{l+2, l+4, \ldots, l+2N\} \\ |u_i| &\ge |u_{i+1}|, \forall i \in \{l+1, l+3, \ldots, l+2N-1\} \end{aligned}\right\} \quad (8c) \\
&\left.\begin{aligned} V_{t,i} &\le V_{max}, \forall i \in \{l+1, \ldots, l+2N\} \\ -V_{t,i} &\le -V_{min}, \forall i \in \{l+1, \ldots, l+2N\} \end{aligned}\right\} \quad (8d) \\
&x_{el,k} = x_{el,l},\; x_{th,k} = x_{th,l}
\end{aligned}$$

where $z_k = x_{el,k}(1)$, $\bar{T}_k = x_{th,k}(1)$, $G^d_{el} = V_{ocv}(z_{k-1})C^d_{el}(1)z_{k-1}$, $u = [u_1, \ldots, u_{2N}]'$, and $\tilde{\beta}$ is a relative weight that penalizes changes in SOC. In the above, the vector of control variables, u, is arranged such that odd and even elements correspond to discharging and charging current magnitudes respectively.

The cost function of **P1** strikes a compromise between total increase in the cell's average temperature and penalized loss in state of charge over the entire prediction horizon. Eqns. (8a) and (8b) describe the equality constraints on the temperature and electrical model dynamics in which a superscript 'd' indicates the discrete version of the variable. Cell manufacturers typically specify the voltage operating limit $[V_{min}, V_{max}]$, and the maximum charge and discharge current limits as a function of temperature; Eqns. (8c) and (8d) enforce these constraints.

For ease of implementation, the optimal control problem in Eqn. (8) is re-written as an optimization problem by recursive substitution of the dynamics as follows. Expressing the thermal dynamics, in discrete-time as

$$x_{th,k+1} = A^d_{th}x_{th,k} + B^d_{th}\begin{bmatrix} q_k \\ T_{amb,k} \end{bmatrix},$$

with $q_k = u_k^2 R_s$, it can be seen that,

$$\begin{aligned}
&x_{th,k+2N+1} - x_{th,k+1} = \\
&[(A^d_{th})^{2N} - \mathbb{I}_n]x_{th,k+1} + \sum_{j=1}^{2N}(A^d_{th})^{j-1}B^d_{th}\begin{bmatrix} R_s u_p^2 \\ T_{amb,p} \end{bmatrix}
\end{aligned}$$

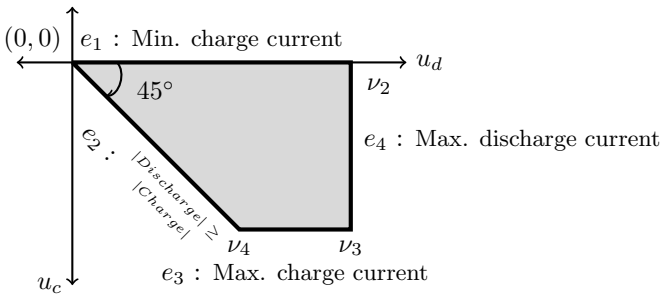

Fig. 6. Region of the constrained optimization problem when the prediction length is one.

where $p = 2N - j + k + 1$.
Then,

$$\begin{aligned}
&\bar{T}_{k+2N+1} - \bar{T}_{k+1} = \underbrace{[1 \quad 0]}_{\tilde{C}}[x_{th,k+2N+1} - x_{th,k+1}], \\
&= \tilde{C}[(A^d_{th})^{2N} - I]x_{th,k} + \tilde{C}\sum_{j=1}^{2N}(A^d_{th})^{j-1}B^d_{th}\begin{bmatrix} R_s u_p^2 \\ T_{amb,p} \end{bmatrix}, \\
&= u'Wu + \text{const.}, \qquad (9)
\end{aligned}$$

where, defining $\vartheta_j := \tilde{C}(A^d_{th})^{2N+k-j}B^d_{th}\tilde{C}'R_s$, $W = diag([\vartheta_1, \ldots, \vartheta_{2N}])$. The constant term in Eqn. (9) can be expressed as $\tilde{C}[(A^d_{th})^{2N} - I]x_{th,k} + \bar{C}\sum_{j=1}^{2N}(A^d_{th})^{j-1}B^d_{th}\bar{C}T_{amb,2N-j+k+1}$ where $\bar{C} = [0\ 1]$. As constant terms in the cost are immaterial to minimization problems, the above constant is dropped in the following expressions.

Since the evolution of SOC is related to the summation of the control variables, the original problem in Eqn. (8) can be re-written in the following form

$$\begin{aligned}
&\min_{u} \; -\|u\|^2_W + \beta\sum_j u_j \\
&\text{subject to : } \Psi u \le \Upsilon \\
&\qquad |u_i| \le |I_d(\bar{T})|, \forall i \in \{1, 3, \ldots, 2N-1\} \\
&\qquad |u_i| \le |I_c(\bar{T})|, \forall i \in \{2, 4, \ldots, 2N\} \\
&\qquad |u_i| \ge |u_{i+1}|, \forall i \in \{1, 3, \ldots, 2N-1\}
\end{aligned} \qquad (10)$$

where Ψ and Υ are as defined in Eqns. (11) and (12). The above optimization problem belongs to the class of problems where a concave function is minimized over a convex set; such problems have been studied extensively in literature. Solvers of concave optimization problems can be broadly classified as being either approximate or global; global methods generally employ cutting-plane and or branch and bound techniques [26], [27]. In general global solvers are computationally expensive and thus their use may be limited to small-scale problems.

To gain better insight into the nature of the optimization problem under investigation, consider the simple case when the prediction horizon is of length one. Figure 6 presents the characteristic shape of the constraint polytope in $\mathbb{R}^2$ wherein coordinates of the vertices represent, in sequence, the magnitude of discharge and charge pulses. While edge e_1 enforces the trivial condition that charging and discharging pulses cannot have the same polarity, edge e_2 ensures that the magnitude of

This article has been accepted for publication in a future issue of this journal, but has not been fully edited. Content may change prior to final publication. Citation information: DOI 10.1109/TIE.2016.2523440, IEEE Transactions on Industrial Electronics

Algorithm 1: Control Algorithm (open-loop)

```
set flag=0;
set [u_d, u_c]' = [-1, 1]';
set number_of_samples_in_block;
while !flag do
    Compute P_cap;
    if P_cap <= P_dmd then
        Solve optimization problem;
        set [u_d, u_c]' = [-u_d*, u_c*]';
        wait(t_s · number_of_samples_in_block) seconds
    else
        set flag=1;
    end
end
```

† Variables with an '*' superscript are optimal solutions.

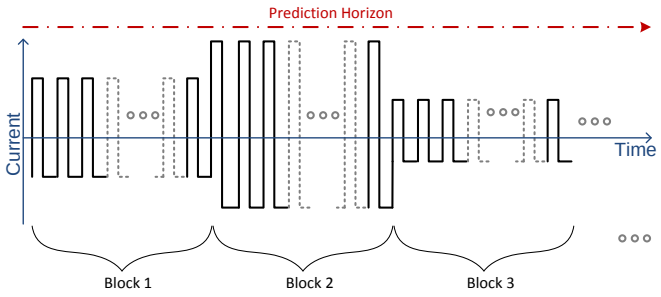

Fig. 7. Blockwise implementation of the MPC problem

the charge current is never greater than that of the discharge current. Edges e_3 and e_4 complete the polytope and enforce adherence to voltage and current constraints.

The bounded polytope defined by constraints in the problem under consideration is convex. The solution to concave minimization problems, when restricted to a convex polytope lies, at one of the vertices of the polytope [28]. For the simple case depicted in Fig. 6, it can be shown that the solution lies at either ν_3 or ν_4. As this work is a feasibility study in a simulation framework, the concave minimization problem is solved using a vertex enumeration strategy to find the global minimizer.

B. Control scheme

In the preceding sub-section, the problem of determining the magnitude of input current of the cell was formulated as an optimization problem in a receding horizon framework. Incorporating the termination condition based on power capability, the overall process can be cast into the control scheme depicted in Alg. 1.

The time constant of the thermal dynamics of the cell under consideration is in the order of tens of minutes. Thus, the increase in temperature as a result of applying one period of current (at 10Hz) may not be significant. For this reason the problem of current magnitude determination is solved in blocks. Periods in the prediction horizon are binned into blocks, with each block consisting of a pre-set number of pulse periods; the prediction horizon is then described by the number of blocks (refer Fig. 7). The optimization problem as formulated earlier is modified to enforce the constraint that every period in each block is identical.

In the overall scheme, at each control instant, the power capability, P_{cap}, is first estimated and compared to the desired set-point, P_{dmd}. If the required power cannot be provided, the optimization problem to compute the magnitudes of the pulses is solved and the optimal solution to the first block is applied. After waiting a duration that is equal to the duration of the block, the process is repeated and the power capability is re-computed. Once the desired power can be delivered, the warm-up operation is terminated.

Remark : Operation of this kind can be interpreted as intentionally allowing the states of the thermal model to grow. The thermal dynamics of a Li-ion cell is inherently stable, unless the temperature is increased to levels that may trigger thermal run-away. It can be argued that given the coupling between the thermal and electrical sub-models, as long as the maximum temperature is bounded away from (from above) a critical temperature ($\approx 80^{\circ}C$), the thermal model remains stable and controllable. As for the electrical dynamics, SOC is a constrained state and the value of V_1 is implicitly bounded as a function of constraints on the terminal voltage and input

$$\Psi = \begin{bmatrix} -D_{el}^d & 0 & 0 & \cdots & 0 \\ C_{el}^d B_{el}^d & D_{el}^d & 0 & \cdots & 0 \\ -C_{el}^d A_{el}^d B_{el}^d & -C_{el}^d B_{el}^d & -D_{el}^d & \cdots & 0 \\ \vdots & \vdots & \vdots & \ddots & \vdots \\ C_{el}^d (A_{el}^d)^{(2N-2)} B_{el}^d & C_{el}^d (A_{el}^d)^{(2N-3)} B_{el}^d & C_{el}^d (A_{el}^d)^{(2N-4)} B_{el}^d & \cdots & D_{el}^d \end{bmatrix} \tag{11}$$

$$\Upsilon = \begin{bmatrix} -V_{min} \\ V_{max} \\ -V_{min} \\ \vdots \\ V_{max} \end{bmatrix} - \begin{bmatrix} -C_{el}^d A_{el}^d \\ C_{el}^d (A_{el}^d)^2 \\ -C_{el}^d (A_{el}^d)^3 \\ \vdots \\ C_{el}^d (A_{el}^d)^{2N} \end{bmatrix} x_k - \begin{bmatrix} -C_{el}^d B_{el}^d \\ C^d A^d B_{el}^d \\ -C_{el}^d (A_{el}^d)^2 B_{el}^d \\ \vdots \\ C_{el}^d (A_{el}^d)^{2N-1} B_{el}^d \end{bmatrix} u_k - \begin{bmatrix} -(V_{ocv}(z_k) - C_{el}^d(1) z_k) \\ V_{ocv}(z_k) - C_{el}^d(1) z_k \\ -(V_{ocv}(z_k) - C_{el}^d(1) z_k) \\ \vdots \\ V_{ocv}(z_k) - C_{el}^d(1) z_k \end{bmatrix} \tag{12}$$

$W = diag([\vartheta_1, \ldots, \vartheta_{2N}])$, $\vartheta_i > 0$, ϑ_i are functions of thermal system matrices.

This article has been accepted for publication in a future issue of this journal, but has not been fully edited. Content may change prior to final publication. Citation information: DOI 10.1109/TIE.2016.2523440, IEEE Transactions on Industrial Electronics

current.

V. Simulation and Discussion

In this section, the proposed Pulsed Current Method (PCM) is simulated with both the plant and model dynamics dictated by the equations in Section II.

A. Simulation Setup

The augmented electro-thermal model (Eqn. (13)) is nonlinear in input and output; the proposed algorithm is implemented using discrete local linear models and is simulated in the MATLAB/Simulink environment using a custom vertex enumerator.

$$\begin{bmatrix}\dot{x}_{el}\\ \dot{x}_{th}\end{bmatrix} = \begin{bmatrix}A_{el}x_{el}\\ A_{th}x_{th}\end{bmatrix} + \begin{bmatrix}B_{el} & 0\\ 0 & B_{th}\end{bmatrix}\begin{bmatrix}u\\ u^2\\ T_{amb}\end{bmatrix}$$
$$V_t = V_{OCV}(x_{el}) + C_{el}x_{el} + D_{el}u, \qquad (13)$$

where u is the current drawn from the cell.

In implementing PCM variable values were chosen as follows – the cell operating voltage bounds were set at $[2, 3.6]$; the frequency of the pulse train was set to 10Hz based on electrochemical considerations [21] and the model was simulated at Nyquist frequency. The energy that is removed from the cell is assumed to be stored in an external storage system such as an ultracapacitor bank.

TABLE II
Manufacturers specifications for A123 26650 cells for constant operation.

Direction	Temperature	Continuous Current
Charge	0–20^{o}C	3A
Charge	20–50^{o}C	10A
Discharge	-30–60^{o}C	60A

The simulated LFP cell is assumed to be a part of a pack that consists of 60 cells in series and four cells in parallel with a rated nominal continuous power at 25°C of 45 kW. Limits on the maximum deliverable current were set by factoring in manufacturers specifications (Table II) and the standards proposed by USABC [29]. Note that the specifications provided in Table II are for continuous discharge. For pulsed currents, a multiplicative factor of 1.5 is used to amplify the current ratings for constant operation. The value of charge current limit below freezing was not provided explicitly in specification sheets. In practice, this limit may have to be empirically estimated if it is not provided. The value of the limit can be taken at the maximum magnitude of current that does not increase the effective resistance of the cell after a pre-determined number of energy cycles (using pulsed currents). In this study this limit is set at 1C. In addition, we assume a Arrhenius relation for the increase in charge current limit above 0°C.

The control scheme proposed in Section IV relies on a receding horizon controller. In receding horizon controllers, the length of the prediction horizon is a tuning parameter that takes integer values. However, for large problems and problem with fast dynamics, shorter control and prediction horizons are preferred; in [30], the authors provide necessary conditions for when the prediction horizon of length one is near optimal. In this section, unless stated otherwise, it assumed that the prediction and control lengths are of length one; the impact of this assumption is studied numerically in Section V-B.

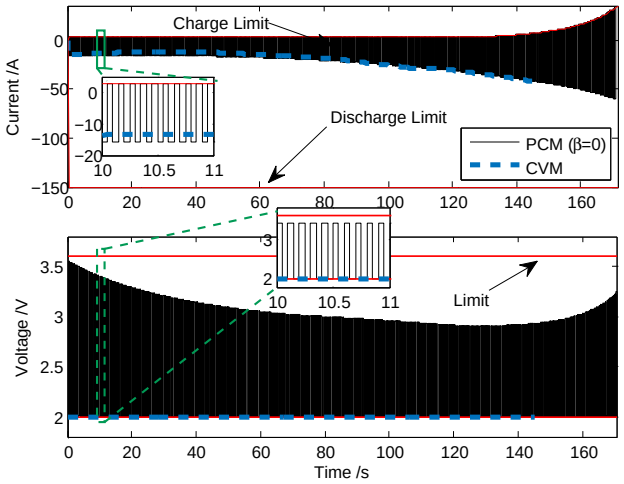

Fig. 8. Down-sampled simulated trajectory of (down-sampled by 19) voltage and current using Pulse Current Method ($\beta = 0$)

B. Simulation, Results & Discussion

This section documents result of simulating the electro-thermal model of the battery developed in Sections II and III using the algorithm described in Section IV. Simulations are run with the following parameters – $SOC_0 = 0.6$, ambient temperature set to -20^oC and under natural cooling condition ($h = 5\,W/m^2K$).

Baseline

To study the performance of the proposed method and to establish a baseline, we compare the trajectories of battery temperature, power capability and SOC from the following two cases:

1) the limiting case when $\beta = 0$
2) the case of maximum permissable continuous discharge.

The second case, when the maximum permissable continuous discharging current is drawn, generates the maximum possible heat at every sample and hence is an approximate solution to the minimum warm-up time problem. In this mode of operation, to satisfy constraints, the terminal voltage is held at V_{min} (that is as long as the discharge current constraint is satisfied); thus, this mode is labeled Constant Voltage Method (CVM).

Figures 8 and 9 present trajectories resulting from simulating the electro-thermal model using the proposed reference current generation algorithm, PCM, and CVM using power demand, ($P_{dmd} = 100$ W) as terminal constraint. Table III tabulates some of the key indices from having applied CVM and PCM.

The value of penalty on SOC lost in each period, β, influences the duration of the warm-up operation. Larger penalties will tend to increase the duration of the warm-up phase; this follows by observing that when operating from

This article has been accepted for publication in a future issue of this journal, but has not been fully edited. Content may change prior to final publication. Citation information: DOI 10.1109/TIE.2016.2523440, IEEE Transactions on Industrial Electronics

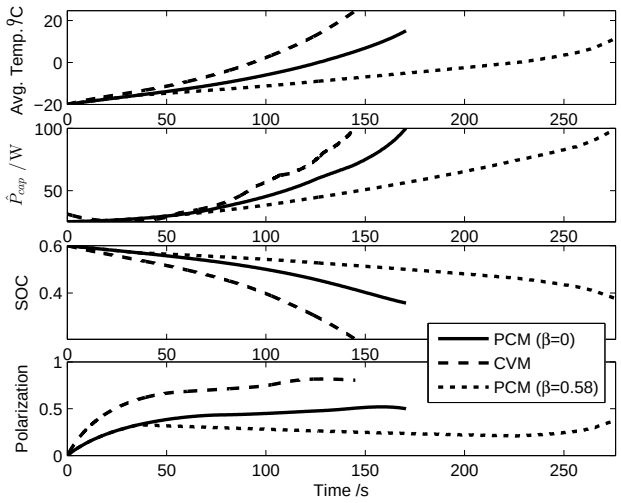

Fig. 9. Simulated trajectories of average temperature, power capability and polarization using Pulse Current Method (PCM) and Constant Voltage (CVM) Method. The simulation was performed with the pack initialized with $SOC_0 = 0.6$ operating from $-20°$C with a terminal power demand, $P_{dmd} = 100$W under natural cooling conditions ($h = 5\ W/m^2K$).

sub-zero temperatures, the current limits are not symmetric. That is, the minimum warm-up time that can be achieved using PCM is when $\beta = 0$. From Fig. 8 and Table III, it is noted that the warm-up time when using CVM is shorter than when using PCM with $\beta = 0$. Thus, the warm-up time using PCM, for any value of β, will be longer than when using CVM.

Energy storage elements such as ultra-capacitors do not have very high energy densities, i.e., it is desirable to transfer as little energy as possible to the external energy storage element. From Table III, note that the equivalent SOC stored in external storage using CVM is almost twice that of PCM.

Lastly, in comparing the effective energy lost using both methods — PCM and CVM — it is noted that CVM is more lossy. More specifically, comparing the CVM with PCM ($\beta = 0$), we observe that the total energy lost increases by nearly 35%; this increased loss manifests itself as increased terminal temperature of the cell.

The above results bear evidence to the fact that terminating warm-up based on terminal temperature is not the same as when using power as terminal constraint. While CVM enjoys shorter operating times, it is more lossy and requires larger storage elements as compared to PCM.

Penalizing energy loss

As formulated, the value of penalty β in the cost can be used to regulate the amount of energy dissipated as heat. Figure 10 documents the total energy lost and the reduction in size of external storage elements in equivalent battery SOC, for different values of β. Inspecting Fig. 10, it it evident that increasing the value of β can reduce energy expenditure and external sizing. By computing the percent change with respect to when $\beta = 0$, the energy lost and external storage size can be reduced by as much as 20%. This increased efficiency of operation does however come at the expense of operation time. Figure 11 presents a comparison between the increase in warm-up efficiency and time taken to be able to deliver the desired power; increased energy efficiencies result in increasing warm-up times.

TABLE III
COMPARISON BETWEEN PCM* AND CVM, KEY INDICES

Method	Oper. Time	SOC_{store}	T_{final}	SOC_{loss}
PCM ($\beta = 0$)	172s	0.13	17.5^{o}C	0.11
PCM ($\beta = 0.58$)	278s	0.12	12.25^{o}C	0.10
CVM	143s	0.23	24.3^{o}C	0.15

*1 block with 5 periods

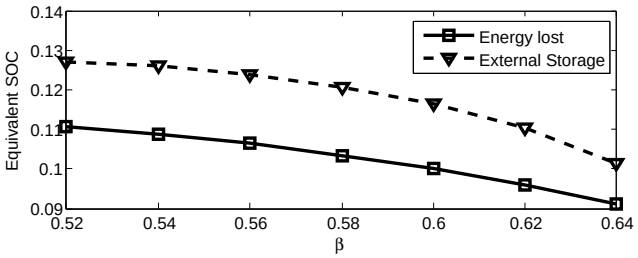

Fig. 10. Results on increasing penalty on energy loss as percent of when no penalty is applied. The simulation was performed with the pack initialized with $SOC_0 = 0.6$ operating from $-20°$C with a terminal power demand, $P_{dmd} = 100$ W under natural cooling conditions ($h = 5\ W/m^2K$).

The observations from Figs. 10 and 11 can be explained by studying the trajectories of terminal and polarization voltages, when $\beta = 0$ and $\beta = 0.58$; Figs. 9 and 12 depict these trajectories. The first observation from comparing these figures is that unlike the case when $\beta = 0$, the trajectory of terminal voltage when $\beta = 0.58$, does not always hit the lower limit of 2V; however, it does on occasion. Further, the trajectory of polarization is different after 40 s; these observations can be interpreted as follows.

From the problem formulation in Eqn. (10), it is possible to show that the value of polarization and the cell's operating temperature result in the solution migrating between vertices of the constraint polytope (as an example cf. Fig. 6 and vertices ν_3 and ν_4). The vertices between which the solution switches are dictated by the temperature of the cell, penalty β and the polarization. As the penalty, β, increases, SOC lost over the control horizon becomes important; therefore, the optimal solution tends to be $u_d = u_c$, i.e. the amplitudes of current during charge and discharge are the same, which can be clearly observed in Fig. 11 when $\beta = 0.58$ compared to the case of $\beta = 0$ in Fig. 9. The preference of charging and discharging

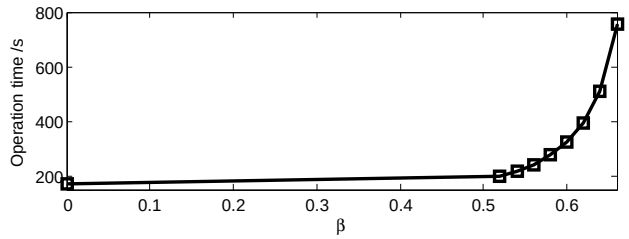

Fig. 11. Comparison between increased efficiency and warm-up operation time

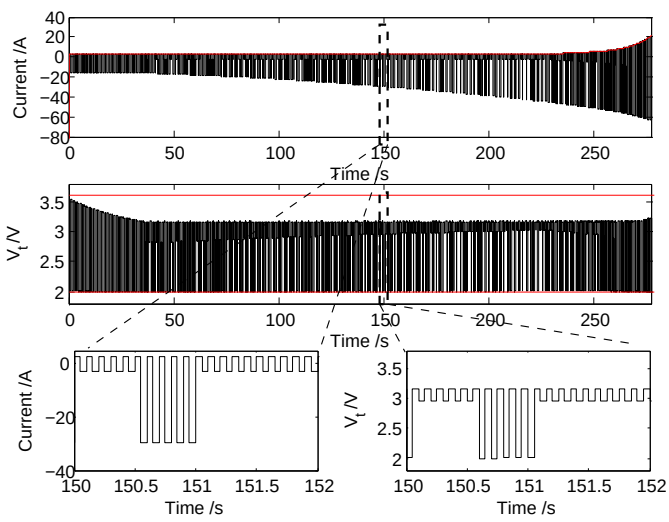

Fig. 12. Simulated trajectory of voltage, polarization and current using Pulse Current Method, $\beta = 0.58$. The simulation was performed with the pack initialized with $SOC_0 = 0.6$ operating from -20°C with a terminal power demand, $P_{dmd} = 100$W under natural cooling conditions ($h = 5\ W/m^2K$).

at the same current rate has to consequences:

1) the average current during the control horizon decreases to zero and hence polarization voltage drops as well.
2) the heat generated during each period reduces and correspondingly the increasing rate of temperature diminishes.

As seen from Fig. 8, the increasing rate of temperature becomes lower when $\beta = 0.58$ than when no penalty on SOC loss is imposed. It is also observed that polarization voltage decreases from 50 second to 230 second. The polarization state is inherently stable; as the average current during each block in the control horizon tends to zero, the value of polarization decreases. The reduced polarization and rate of heat generation may result in the solution switching back to the vertex that extracts maximum current from the cell (vertex ν_3 in Fig. 6). This results in the switching behavior observed in Fig. 12.

Figure 11 also highlights another important characteristic of the solution – as the value of β is increased, the operation time reaches an asymptote, i.e. it becomes impossible to reach the desired terminal power capability. This is an extension of the behavior described above wherein the solution migrates; as β increases, the solution migrates and remains at the vertex that favors charging and discharging currents being of the same magnitude (vertex ν_4 in Fig. 6). In addition, for βs sufficiently large, the solution will remain at the vertex that favours negligible SOC loss and hence the power demand can never be achieved. Thus, for the above algorithm to be implemented, the value of β needs to be chosen appropriately to ensure feasibility of the overall problem.

Effect of longer prediction horizons

In simulating the results presented thus far, the prediction horizon was set to be a single block consisting of five pulses. In the context of predictive control, longer prediction horizons are known to produce better approximations of the global optimal solution. In this application, owing to the linearized MPC implementation, the prediction horizon cannot be taken to be arbitrarily large without incurring errors resulting from model linearization.

[1]Simulations were performed on a computer powered by an Intel i5-2500 quad-core processor with 16GB of ram and running Windows 7 with parallelization enabled.

TABLE IV
IMPACT OF PREDICTION HORIZON BASED ON KEY INDICES*

Index \ Prediction Length	1	2	3
SOC_{loss}	1	0.99	0.98
External Storage	1	0.99	0.97
Terminal Time	1	1.01	1.03
Computational Time	1	35	107

* Entries normalized wrt. results when prediction length is one block

To investigate the influence of prediction horizon on the optimal solution trajectory, an iterative test was performed[1]wherein the length of the prediction horizon was increased incrementally; results of which are presented in Table IV. The other parameters of the simulation were : $P_{dmd} = 50W$, $h = 5W/m^2K$ and $\beta = 0.57$ (the power demand is set at 50 W in the interest of computational time).

The data presented in Table IV, as expected, indicates that given the same penalty on loss in energy, increasing the length of the prediction horizon decreases the total energy lost; this however does come at the expense of computational time. In fact, there appears to be a quadratic relation between decrease in loss and total operation-time. Comparing the effective increase in savings and the increase in computational and operation time, a case for the use of prediction horizon of length one block can be made.

VI. CONCLUSION

In this work, a Li-ion battery warm-up strategy that increases the cell temperature to meet power demand in an energy efficient method is described. The shape of current used to shuttle energy between the cell and an external energy storage system was set to be bi-directional pulses to minimize polarization and reduce damage to electrodes. Magnitude of the pulses were determined by solving a constrained optimization problem. From simulations based on models of a 26650 LFP cell, it is noted that it is possible to reduce energy lost as heat and the size of external storage, by as much as 20% when compared against using just constant voltage discharge. There is however, a compromise to be made between reduction in size of storage, energy lost and time taken to warm-up. A future work will study the impact of the proposed technique experimentally and ascertain if the conclusion in [31]—that pulsed currents can accelerate degradation—is indeed applicable to operations of the kind considered in this study.

REFERENCES

[1] A. Affanni, A. Bellini, G. Franceschini, P. Guglielmi, and C. Tassoni, "Battery choice and management for new-generation electric vehicles," *IEEE Trans. Ind. Electron.*, vol. 52, no. 5, pp. 1343–1349, Oct 2005.
[2] H. Rahimi-Eichi, U. Ojha, F. Baronti, and M. Chow, "Battery management system: An overview of its application in the smart grid and electric vehicles," *IEEE Trans. Ind. Electron.*, vol. 7, no. 2, pp. 4–16, June 2013.

[3] S. Mohan, Y. Kim, A. Stefanopoulou, and Y. Ding, "On the warmup of li-ion cells from sub-zero temperatures," in *American Control Conference (ACC), 2014*, June 2014, pp. 1547–1552.
[4] Y. Ji, Y. Zhang, and C.-Y. Wang, "Li-ion cell operation at low temperatures," *Journal of The Electrochemical Society*, vol. 160(4), pp. 636–649, 2013.
[5] Z. Rao and S. Wang, "A review of power battery thermal energy management," *Renewable and Sustainable Energy Reviews*, vol. 15, no. 9, pp. 4554 – 4571, 2011.
[6] X. Zhang, X. Kong, G. Li, and J. Li, "Thermodynamic assessment of active cooling/heating methods for lithium-ion batteries of electric vehicles in extreme conditions," *Energy*, vol. 64, no. 0, pp. 1092 – 1101, 2014.
[7] H. Baba, K. Kawasaki, and H. Kawachi, "Battery heating system for electric vehicles," SAE Technical Paper, Tech. Rep., 2015.
[8] A. Pesaran, A. Vlahinos, and T. STUART, "Cooling and preheating of batteries in hybrid electric vehicles," in *The 6th ASME-JSME Thermal Engineering Joint Conference*, 2003.
[9] T. Stuart and A. Hande, "HEV battery heating using ac currents," *Journal of Power Sources*, vol. 129, no. 2, pp. 368 – 378, 2004.
[10] Y. Ji and C. Y. Wang, "Heating strategies for Li-ion batteries operated from subzero temperatures," *Electrochimica Acta*, vol. 107, pp. 664 – 674, 2013. [Online]. Available: http://www.sciencedirect.com/science/article/pii/S0013468613005707
[11] Y. Kim, S. Mohan, J. B. Siegel, and A. G. Stefanopoulou, "Maximum power estimation of lithium-ion batteries accounting for thermal and electrical constraints," in *ASME 2013 Dynamic Systems and Control Conference*, vol. 2, October, 2013.
[12] Y.-H. Liu and Y.-F. Luo, "Search for an optimal rapid-charging pattern for li-ion batteries using the taguchi approach," *IEEE Trans. Ind. Electron.*, vol. 57, no. 12, pp. 3963–3971, Dec 2010.
[13] J. Jiang, Q. Liu, C. Zhang, and W. Zhang, "Evaluation of acceptable charging current of power li-ion batteries based on polarization characteristics," *IEEE Trans. Ind. Electron.*, vol. 61, no. 12, pp. 6844–6851, Dec 2014.
[14] J. Fan and S. Tan, "Studies on charging lithium-ion cells at low temperatures," *Journal of The Electrochemical Society*, vol. 153 (6), pp. A1081–A1092, 2006.
[15] S. Zhang, K. Xu, and T. Jow, "A new approach toward improved low temperature performance of li-ion battery," *Electrochemistry Communications*, vol. 4, no. 11, pp. 928 – 932, 2002.
[16] L.-R. Chen, S.-L. Wu, D.-T. Shieh, and T.-R. Chen, "Sinusoidal-ripple-current charging strategy and optimal charging frequency study for li-ion batteries," *IEEE Trans. Ind. Electron.*, vol. 60, no. 1, pp. 88–97, Jan 2013.
[17] M. Doyle, T. F. Fuller, and J. Newman, "Modeling of galvanostatic charge and discharge of the lithium/polymer/insertion cell," *Journal of Electrochemical Society*, vol. 140(6), pp. 1526–1533, 1993.
[18] A. P. Schmidt, M. Bitzer, rpd W. Imre, and L. Guzzella, "Experiment-driven electrochemical modeling and systematic parameterization for a lithium-ion battery cell," *Journal of Power Sources*, vol. 195, no. 15, pp. 5071 – 5080, 2010.
[19] X. Lin, H. E. Perez, S. Mohan, J. B. Siegel, A. G. Stefanopoulou, Y. Ding, and M. P. Castanier, "A lumped-parameter electro-thermal model for cylindrical batteries," *Journal of Power Sources*, vol. 257, no. 0, pp. 1 – 11, 2014.
[20] W. Huang and J. Qahouq, "An online battery impedance measurement method using dc-dc power converter control," *IEEE Trans. Ind. Electron.*, vol. 61, no. 11, pp. 5987–5995, Nov 2014.
[21] S. Tippmann, D. Walper, L. Balboa, B. Spier, and W. G. Bessler, "Low-temperature charging of lithium-ion cells part I: Electrochemical modeling and experimental investigation of degradation behavior," *Journal of Power Sources*, vol. 252, pp. 305 – 316, 2014.
[22] X. Hu, R. Xiong, and B. Egardt, "Model-based dynamic power assessment of lithium-ion batteries considering different operating conditions," *IEEE Trans. Ind. Informat.*, vol. 10, no. 3, pp. 1948–1959, Aug 2014.
[23] Y. Kim, S. Mohan, J. Siegel, A. Stefanopoulou, and Y. Ding, "The estimation of temperature distribution in cylindrical battery cells under unknown cooling conditions," *IEEE Trans. Control Syst. Technol.*, vol. 22, no. 6, pp. 2277–2286, 2014.
[24] L.-R. Chen, J.-J. Chen, C.-M. Ho, S.-L. Wu, and D.-T. Shieh, "Improvement of li-ion battery discharging performance by pulse and sinusoidal current strategies," *IEEE Trans. Ind. Electron.*, vol. 60, no. 12, pp. 5620–5628, Dec 2013.
[25] S. Burer and A. N. Letchford, "Non-convex mixed-integer nonlinear programming: A survey," *Surveys in Operations Research and Management Science*, vol. 17, no. 2, pp. 97 – 106, 2012. [Online]. Available: http://www.sciencedirect.com/science/article/pii/S1876735412000037
[26] R. Horst, "On the global minimization of concave functions," *Operations-Research-Spektrum*, vol. 6, no. 4, pp. 195–205, 1984. [Online]. Available: http://dx.doi.org/10.1007/BF01720068
[27] H. P. Benson and R. Horst, "A branch and bound-outer approximation algorithm for concave minimization over a convex set," *Computers & Mathematics with Applications*, vol. 21, no. 67, pp. 67 – 76, 1991. [Online]. Available: http://www.sciencedirect.com/science/article/pii/089812219190161V
[28] R. T. Rockafellar, *Convex analysis*. Princeton university press, 1997.
[29] The Idaho National Laboratory, *Battery Test Manual For Plug-In Hybrid Electric Vehicles*, 2nd ed., U.S. Department of Energy Vehicle Technologies Program, December 2010.
[30] C. Muller, D. E. Quevedo, and G. C. Goodwin, "How good is quantized model predictive control with horizon one?" *IEEE Trans. Autom. Control*, vol. 56, no. 11, pp. 2623–2638, 2011.
[31] F. Savoye, P. Venet, M. Millet, and J. Groot, "Impact of periodic current pulses on li-ion battery performance," *IEEE Trans. Ind. Electron.*, vol. 59, no. 9, pp. 3481–3488, Sept 2012.

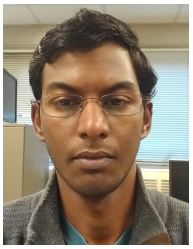

Shankar Mohan received his bachelor's degree from the National University of Singapore in 2011 and his master's degree from the University of Michigan in 2013, both in Electrical Engineering. He is currently working towards a PhD. in Electrical Engineering at the University of Michigan. His current interests include numerical optimization methods and the application of control techniques to energy systems.

Youngki Kim (M'14) is currently a Postdoctoral Research Fellow with the Powertrain Control Laboratory, University of Michigan. He received his B.S. and M.S. degrees in the School of Mechanical and Aerospace Engineering at Seoul National University in 2001 and 2003 respectively, and his Ph.D degree in Mechanical Engineering Department from the University of Michigan in 2014. He worked as a Research Engineer in the R&D Division at Hyundai Motor Company from 2003 to 2008. His research interests include modeling, simulation and optimal control/estimation of dynamic systems such as electrified vehicles and electrochemical energy storage systems.

Anna G. Stefanopoulou (F'09) is a Professor of mechanical engineering and the Director of the Automotive Research Center, University of Michigan, Ann Arbor. From 1998 to 2000, she was an Assistant Professor with the University of California, Santa Barbara. From 1996 to 1997, she was a Technical Specialist with Ford Motor Company. She has authored or co-authored more than 200 papers and a book on estimation and control of internal combustion engines and electrochemical processes such as fuel cells and batteries. She holds nine U.S. patents. Prof. Stefanopoulou is a Fellow of the ASME. She was a recipient of four Best Paper Awards.